

Proceeding Paper

Acoustic Cavitation and Ionic Liquid Combined: A Modeling Investigation of the Possible Promises in Terms of Physico-Chemical Effects [†]

Kaouthier Kerboua

Department of Process and Energy Engineering, National Higher School of Technology and Engineering, Annaba 23005, Algeria; k.kerboua@esti-annaba.dz

[†] Presented at the 4th International Electronic Conference on Applied Sciences, 27 October–10 November 2023; Available online: <https://asec2023.sciforum.net/>.

Abstract: The present work is based on a mathematical model describing a single acoustic cavitation bubble oscillating under an ultrasonic field of 200 and 300 kHz and an acoustic amplitude of 1.8 atm within 1-butyl-3-methylimidazolium acetate. The model integrates the dynamics of bubble oscillation, the thermodynamics applied to the interior of the bubble and at its interface, and the sonophysical and sonochemical events occurring in the presence of dissolved cellulose in the ionic liquid. The performed simulations shed light on the major physical effects of acoustic cavitation, namely the shockwave and microjet, as well as the sonochemical effects in terms of the degradation rate of the dissolved cellulose in the secondary reactional site, i.e., the interface. The predominance of the effects and its dependency of the acoustic frequency is tackled from an energetic point of view. It is demonstrated that 300 kHz offers the lowest heat flow across the bubble interface, lowering the chances for the sonochemical degradation of cellulose, while 200 kHz offers a significant degradation rate, attaining $71.4 \text{ mol}\cdot\text{dm}^{-3}\cdot\text{s}^{-1}$, as well as harsher microjets and shockwaves with powers of 3300 and 900 mW at collapse, respectively.

Keywords: ultrasounds; acoustic cavitation; [C4mim][CH3COO]; cellulose; temperature; pressure; sonochemistry; microjet; shockwave



Citation: Kerboua, K. Acoustic Cavitation and Ionic Liquid Combined: A Modeling Investigation of the Possible Promises in Terms of Physico-Chemical Effects. *Eng. Proc.* **2023**, *56*, 237. <https://doi.org/10.3390/ASEC2023-16313>

Academic Editor: Elisabeta Szerb

Published: 21 November 2023



Copyright: © 2023 by the author. Licensee MDPI, Basel, Switzerland. This article is an open access article distributed under the terms and conditions of the Creative Commons Attribution (CC BY) license (<https://creativecommons.org/licenses/by/4.0/>).

1. Introduction

Several researchers have described the dissolution of cellulose in ionic liquid and have offered diverse molecular theories. Most of them agree that cellulose dissolves when anions make hydrogen bonds with it, but others have demonstrated that cellulose dissolves in ionic liquids when an anion and a cation make hydrogen bonds with the hydrogen and oxygen atoms of the cellulose, which are precisely positioned between the C6 and C3 hydroxyl groups of the nearby cellulose chain [1]. Moreover, according to several studies, the exposure of the ionic liquid to ultrasounds revealed some interesting physical and chemical effects that may be beneficial in terms of cellulose degradation [2]. Nonetheless, the joint investigation of the sonophysical and sonochemical effects with this configuration has not yet been performed, particularly through modeling and simulation. The present paper proposes a numerical model describing the behavior of a single acoustic cavitation bubble within [C4mim][CH3COO] in the presence of dissolved cellulose, with the aim to evaluate the chemical and physical impact of sonication, under the specific acoustic frequencies of 200 and 300 kHz, generally adopted in sonochemistry.

2. Numerical Model

1-Butyl-3-methylimidazolium acetate [C4mim][CH3COO] is an ionic liquid characterized by a high cellulose solvation power [3,4]. In the present model, the gaseous medium is saturated with argon. Despite the fact that only a limited number of studies have examined

the solubility of argon in ionic liquids [5–8], the reported solubility rates are judged as sufficient for creating gaseous inclusions and generating acoustic cavitation by a heterogeneous nucleation process [9] when enough tensile strength is induced [10].

The ionic liquid was submitted to ultrasonication at 200 and 300 kHz of frequency, and an acoustic amplitude of 1.8 atm, which is the lowest acoustic amplitude (under the lowest temperature) that allows for the acoustic cavitation phenomenon and consequently the expected chemical effects. The operating temperature was fixed at 353 K to attain an acceptable value of dynamic viscosity of the ionic liquid. The ambient radii at the respective acoustic frequencies were taken as 5 and 3.5 μm. The oscillation of the bubble was governed by the Keller–Miksis equation, as indicated in Equation (1).

$$\ddot{R} = \frac{(c+\dot{R})}{\rho_L(cR-\dot{R}R)+4\mu} \left(P_g - \frac{2\sigma}{R} - 4\mu\frac{\dot{R}}{R} - P_\infty + P_a \sin\left(2\pi f\left(t + \frac{R}{c}\right)\right) \right) + \frac{R}{\rho_L(cR-\dot{R}R)+4\mu} \left(\dot{P}_g + \frac{26\dot{R}}{R^2} + 4\mu\frac{\dot{R}^2}{R^2} \right) - \frac{\rho_L(3c-\dot{R})\dot{R}^2}{2(\rho_L(cR-\dot{R}R)+4\mu)} \tag{1}$$

Safarov et al. [11] provided the physical parameters of 1-butyl-3-methylimidazolium acetate at 353 K in relation to temperature. These properties include surface tension σ , dynamic viscosity μ , density ρ_L , and sound speed c .

Since 1-butyl-3-methylimidazolium acetate has a very low vapor pressure [12], argon was assumed to be the only gas present in the bubbles. The initial pressure of the gas inside the bubble, as determined by the mechanical equilibrium condition, is given by Equation (2).

$$P_{g0} = P_\infty + \frac{2\sigma}{R_0} \tag{2}$$

The energy balance applicable to the acoustic cavitation bubble considering its oscillation is given in Equation (3). It allows for the determination of the variation and distribution of the temperature as a function of time and space.

$$\dot{T} = \frac{1}{nC_V(T)} \left(-P_g 4\pi R^2 \dot{R} - \varphi(t) \right) \tag{3}$$

$\varphi(t)$ represents the heat flow passing through the thermal boundary layer of the width ξ , and its expression is based on the continuity of the thermal flow across the bubble interface at each instant t , as seen in Equation (4).

$$\varphi(t) = \frac{4\pi R(R-\xi)}{\xi} \int_{T(t)}^{T_\infty} \lambda(T) dT \tag{4}$$

The isochoric molar heat capacity of argon $C_V(T)$ and its thermal conductivity $\lambda(T)$, appearing respectively in Equations (3) and (4), vary in function of the temperature of the bulk volume of the bubble. Both are expressed as a polynomial form, as shown in [13].

The pressure of gases inside the bubble volume is expressed using the Van der Waals state equation as shown in Equation (5).

$$\left(P_g + \frac{n^2 a}{V^2} \right) (V - nb) = nR_g T \tag{5}$$

Due to the ionic liquid’s high order of magnitude thermal conductivity, which is almost 10 times higher than that of argon [14,15], the resistance to thermal diffusion is found on the gaseous side. As a result, the boundary layer of thermal diffusion is taken into account on the gaseous side; Equation (6) [16] gives its width ξ . This equation includes the thermal diffusivity κ , which is temperature-dependent and depends on the density, heat capacity, and thermal conductivity of argon.

$$\zeta = \min \left(\sqrt{\frac{R\kappa}{|\dot{R}|}}, \frac{R}{\pi} \right) \tag{6}$$

With the exception of the thin boundary layer with a width ζ [17], it is assumed that the temperature is spatially consistent throughout the majority of the bubble. Resolving Equation (7) yields the radial distribution of temperature throughout the thermal boundary layer (the result of the integration of Equation (4)) for each value of r between 0 and ζ .

$$1.79435 \times 10^5 T(R-r)^2 + 6.81277 \times 10^{-3} T(R-r) - 4.6408 = \frac{r \varphi(t)}{4\pi R(R-r)} \tag{7}$$

The thermal effect caused by the hot spots at the bubble interface (the second reactivity site), according to the two sites model [2], constitutes the seat of chemical reactions. The bubble’s main body is thought to be chemically inert. The cellulose is anticipated to thermally disintegrate in accordance with the process put forward by Diebold [18] and shown in [19], i.e., when the bulk temperature is high enough and the surrounding temperature is adequate to start pyrolysis reactions.

The chemical kinetics occurring in the second reactivity site is described as a chain mechanism of first order reactions, with the molar yield of each species k being controlled by Equation (8).

$$\frac{dn_k}{dt} = V_r \sum_{i=1}^7 (\vartheta'_{ki} - \vartheta_{ki}) A_i e^{\left(\frac{-E_i}{R_g T_r}\right)} \prod_{k=1}^K (c_k)^{\vartheta_{ki}} \tag{8}$$

In this equation, T_r constitutes the temperature governing the chemical kinetics of the decomposition of cellulose. This temperature varies spatially as a function of the bubble radius r , as shown in Equation (7), and the median value is considered to approximate the conditions of the thermal decomposition of cellulose. The molar concentrations c_k of each chemical species k involved in the mechanism are reported in the volume of the thermal boundary layer of width ζ shown previously. This volume is denoted V_r and is given in Equation (9).

$$V_r = \frac{4}{3} \pi \left(R^3 - \left(R - \min \left(\sqrt{\frac{R\kappa}{|\dot{R}|}}, \frac{R}{\pi} \right) \right)^3 \right) \tag{9}$$

When the bubble collapses, a spherical shockwave is generated around the bubble in the liquid medium. This shockwave can provoke changes in the transport properties, by inducing a dispersion of molecules in the liquid phase and consequently promoting mass transfer. The power emitted by the single acoustic cavitation bubble in the form of a shockwave P_s is expressed by Equation (10).

$$P_s = \frac{4\pi\rho_{el}}{c} \left(R^2 \ddot{R} + 2RR\dot{R} \right)^2 \tag{10}$$

Additionally, during the bubble collapse near a solid surface (cellulose particles), the bubble loses its sphericity. A modification of the shape of the bubble is observed from the original approximate sphere to a slender shape and then a flattened shape. At the final stage, a microjet breaks the bubble wall near the solid and impacts towards it. Micro-jet velocity is given by Equation (11) [20].

$$v = 8.97 \left(\frac{R}{R_0} \right)^2 \sqrt{\frac{P_\infty + P_A \sin(2\pi ft) - P_v}{\rho_{el}}} \tag{11}$$

The power of the exit P_j is then shown in Equation (12) as a function of the jet velocity v and the jet nozzle exit diameter h (taken as a third of the value of the bubble diameter) [21,22].

$$P_j = \frac{1}{8} \pi \rho_{el} h^2 v^3 \tag{12}$$

The system of non-linear and dependent differential equations (Equations (1), (3), and (8)) is simultaneously resolved with the non-linear equations (Equations (4)–(9)) using the Ode23s solver of Matlab. The shockwave and microjet powers are then assessed according to Equations (10) and (12).

3. Results and Discussion

3.1. Dynamics of Oscillation of the Acoustic Cavitation Bubble

Figure 1a shows the evolution of the argon bubble radius within the sonicated ionic liquid $[\text{C}_4\text{min}][\text{CH}_3\text{COO}]$ under both 200 and 300 kHz frequencies.

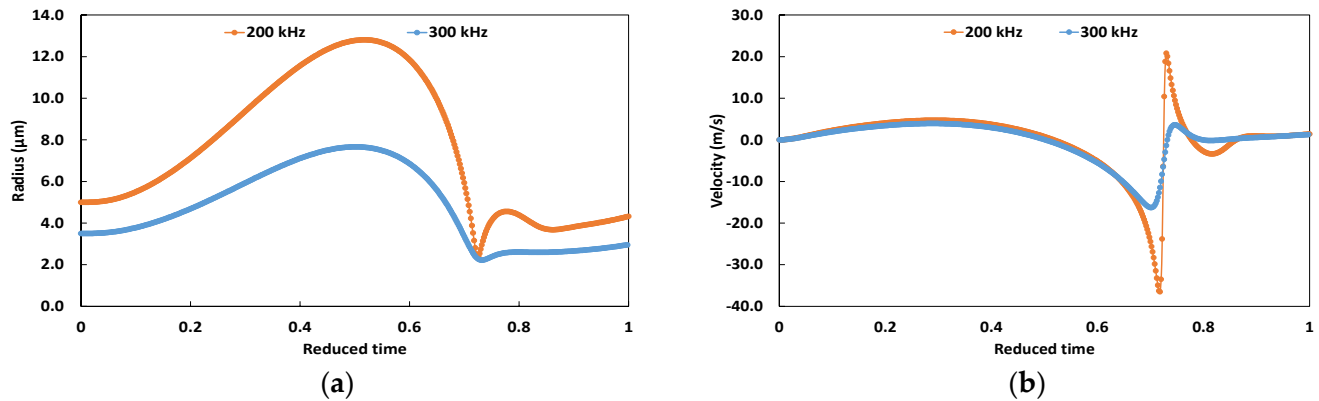


Figure 1. Bubble radius (left (a)) and wall velocity (right (b)) as functions of reduced times under 200 and 300 kHz.

The results demonstrate that a 200 kHz frequency induces a harsher oscillation of the bubble wall, achieving a maximum radius of almost 13 μm , with an expansion ratio of 2.6, vs. 2.18 under 300 kHz. During the collapse phase, the bubble contracts 3.81 folds under 200 kHz and 3.45 folds under 300 kHz. This trend is confirmed by the evolution of the bubble wall velocity shown in Figure 1b, attaining two extremums of 36.5 and 20 m/s at expansion and collapse, respectively, under 200 kHz.

3.2. Thermodynamics of the Acoustic Cavitation Bubble

The evolution of the bulk and interfacial temperatures is shown in Figure 2. As predicted from the dynamics of the bubble oscillation, the highest temperature was attained under 200 kHz, with 1600 K in the bulk volume and 1000 K at the interface, at the moment of collapse. A 300 kHz frequency barely leads to 474 K at the interfacial zone, which limits the sonochemical activity there under this acoustic condition.

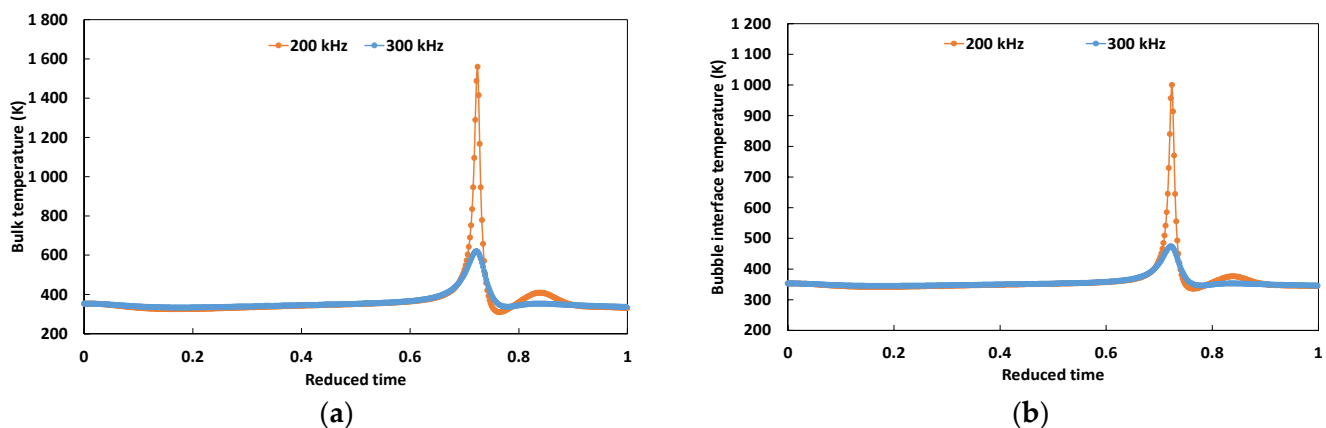


Figure 2. Bulk (left (a)) and interfacial (right (b)) temperatures as functions of reduced time under 200 and 300 kHz.

As a result of the radius and temperature evolutions reported earlier, we noticed that the highest bulk pressure was attained under 200 kHz with a value of 48 bar, as shown in Figure 3. Though the bulk pressure does not directly affect the sonochemical process of cellulose transformation, it shows that a 200 kHz frequency is more favorable for the sonochemical decomposition of cellulose within the sonicated ionic liquid. This point will be further discussed in the following section.

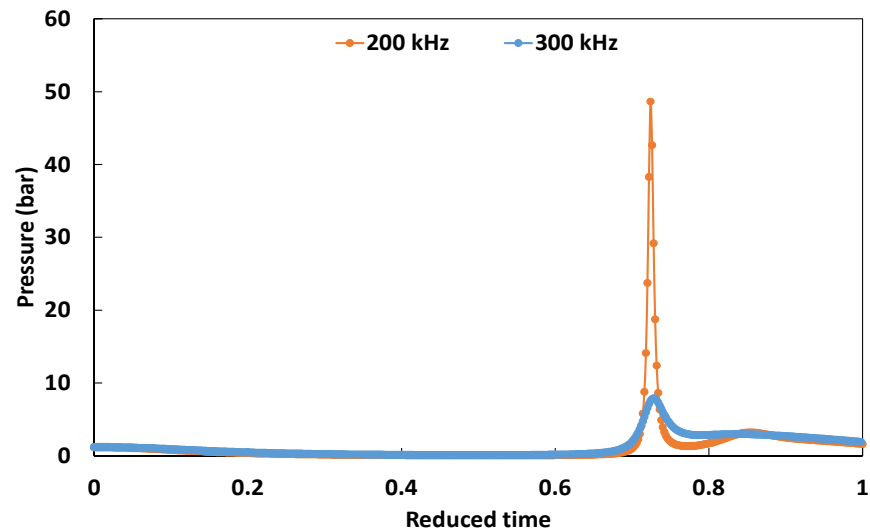


Figure 3. Bulk volume pressure under 200 and 300 kHz.

3.3. Sonochemistry

Figure 4 shows the cellulose decomposition rate the molar yield of cellulose within one acoustic cycle under a 200 kHz frequency. The decomposition rate attains its maximum at the collapse, with a value of $71.4 \text{ mol/dm}^3 \cdot \text{s}$. Though this rate lasts almost $0.05 \mu\text{s}$, it allows the molar yield of cellulose to decrease by 9.77%.

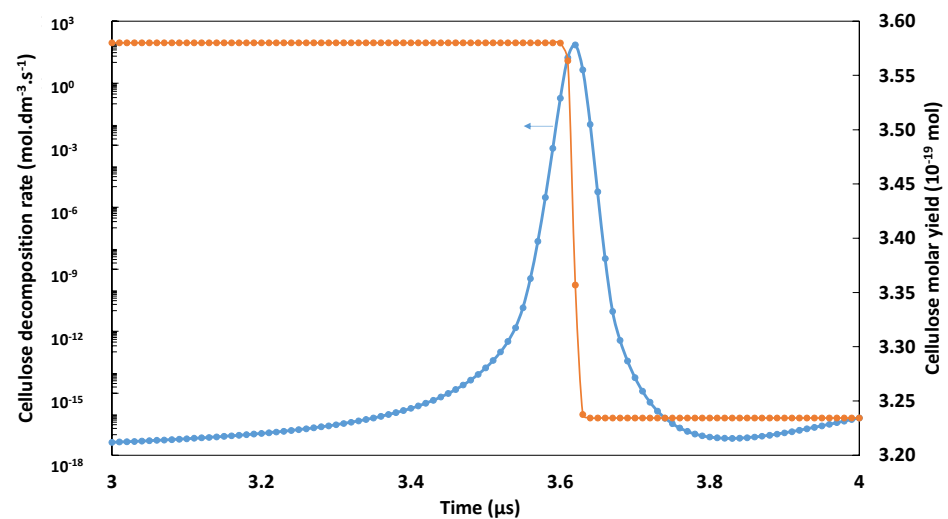


Figure 4. Cellulose decomposition rate and molar yield under 200 kHz.

3.4. Energetic Reading: Heat Transfer, Microjets and Shockwaves

The results related to the thermal flow across the interface exhibit a significantly higher value under 200 kHz, which explains the higher interfacial temperature, as shown in Figure 5a. The interface being the reactional site in the studied case, the prominent sonochemical activity observed under 200 kHz is explained thermally by the more important thermal flow, with a peak exceeding 3 W at collapse (almost 6 folds higher than

at 300 kHz). In terms of the physical effects, 200 kHz also results in harsher induced shockwaves and microjets, with respective peak values of 0.9 and 3.3 W at collapse as shown in Figure 5b,c. Hence, 200 kHz is both sonochemically and sono-physically more promising for the decomposition of cellulose in ionic liquid.

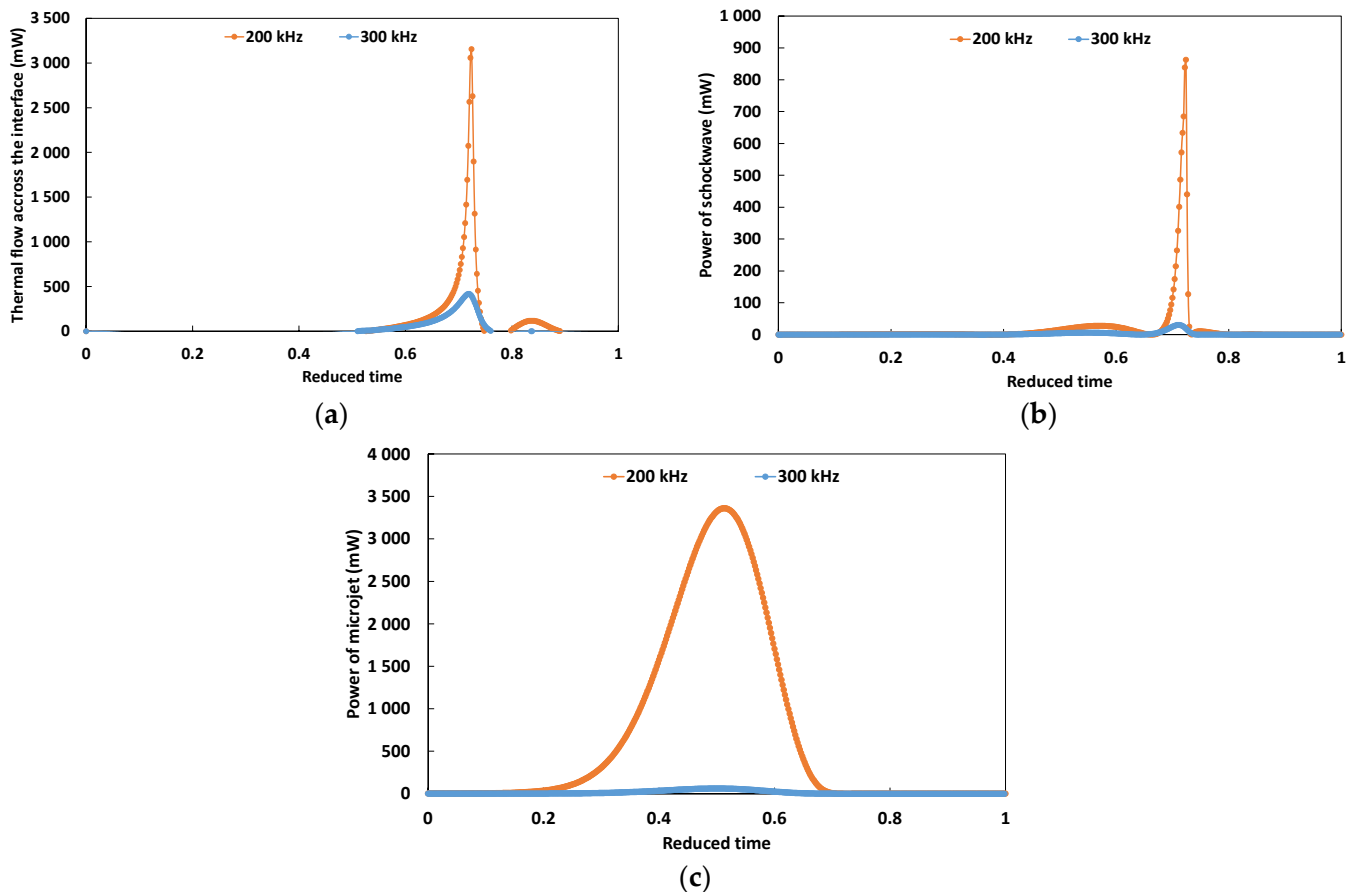


Figure 5. Thermal flow across the interface (upper left (a)), the power of the shockwave (upper right (b)) and the power of the microjet (down (c)) under 200 and 300 kHz.

4. Conclusions

In the present study, the sonochemical and sonophysical effects induced by sonication of the ionic liquid [C4mim][CH₃COO] for the decomposition of cellulose were investigated numerically. The modelling and simulation results revealed that the harsher dynamics of bubble oscillation are achieved under 200 kHz, with expansion and collapse ratios of 2.6 and 3.81, respectively. The trend was confirmed by the bubble wall velocity and resulted in higher temperature values both in the bulk volume of the bubble as well as the interfacial region, which was the sonochemically active zone in the studied case. The simulation of one acoustic cycle revealed that 9.77% of cellulose is decomposed under 200 kHz. The collapse was also accompanied by shockwave and microjet effects, characterized by peak powers of 0.9 and 3.3 W, respectively, per bubble. Finally, 200 kHz sonication was demonstrated to be sonochemically and sonophysically effective for the sono-decomposition of cellulose dissolved in [C4mim][CH₃COO].

Funding: This research received no external funding.

Institutional Review Board Statement: Not applicable.

Informed Consent Statement: Not applicable.

Data Availability Statement: No data was generated.

Acknowledgments: The author acknowledges the support given by the Ministry of Higher Education and Scientific Research in Algeria in the frame of the Project with Social-Economical Impact (PISE 2023) entitled “Green Processes for Sanitation”.

Conflicts of Interest: The author declares no conflict of interest.

References

1. Manna, B.; Ghosh, A. Dissolution of cellulose in ionic liquid and water mixtures as revealed by molecular dynamics simulations. *J. Biomol. Struct. Dyn.* **2019**, *37*, 3987–4005. [[CrossRef](#)]
2. Chatel, G.; Macfarlane, D.R. Ionic liquids and ultrasound in combination: Synergies and challenges. *Chem. Soc. Rev.* **2014**, *43*, 8132–8149. [[CrossRef](#)] [[PubMed](#)]
3. Isik, M.; Sardon, H.; Mecerreyes, D. Ionic liquids and cellulose: Dissolution, chemical modification and preparation of new cellulosic materials. *Int. J. Mol. Sci.* **2014**, *15*, 11922–11940. [[CrossRef](#)] [[PubMed](#)]
4. Xu, A.; Guo, X.; Xu, R. Understanding the dissolution of cellulose in 1-butyl-3-methylimidazolium acetate+DMAc solvent. *Int. J. Biol. Macromol.* **2015**, *81*, 1000–1004. [[CrossRef](#)] [[PubMed](#)]
5. Song, T.; Lubben, M.J.; Brennecke, J.F. Solubility of argon, krypton and xenon in ionic liquids. *Fluid Phase Equilib.* **2020**, *504*, 112334. [[CrossRef](#)]
6. Jacquemin, J.; Costa Gomes, M.F.; Husson, P.; Majer, V. Solubility of carbon dioxide, ethane, methane, oxygen, nitrogen, hydrogen, argon, and carbon monoxide in 1-butyl-3-methylimidazolium tetrafluoroborate between temperatures 283 K and 343 K and at pressures close to atmospheric. *J. Chem. Thermodyn.* **2006**, *38*, 490–502. [[CrossRef](#)]
7. Lee, B.-C.; Outcalt, S.L. Solubilities of Gases in the Ionic Liquid 1-n-Butyl-3-methylimidazolium Bis(trifluoromethylsulfonyl)imide. *J. Chem. Eng. Data* **2006**, *51*, 892–897. [[CrossRef](#)]
8. Anthony, J.L.; Anderson, J.L.; Maginn, E.J.; Brennecke, J.F. Anion Effects on Gas Solubility in Ionic Liquids. *J. Phys. Chem. B* **2005**, *109*, 6366–6374. [[CrossRef](#)]
9. Talanquer, V. Nucleation in gas-liquid transitions. *J. Chem. Educ.* **2002**, *79*, 877. [[CrossRef](#)]
10. Apfel, R.E. Acoustic cavitation. *Methods Exp. Phys.* **1981**, *19*, 355–411. [[CrossRef](#)]
11. Safarov, J.; Geppert-Rybczyńska, M.; Kul, I.; Hassel, E. Thermophysical properties of 1-butyl-3-methylimidazolium acetate over a wide range of temperatures and pressures. *Fluid Phase Equilib.* **2014**, *383*, 144–155. [[CrossRef](#)]
12. Kerboua, K.; Hamdaoui, O.; Alghyamah, A. Acoustic cavitation events and solvation power of ionic liquid in a novel hybrid technique: A concept proposal toward a green pathway for cellulose decomposition. *Ultrason. Sonochem.* **2021**, *73*, 105469. [[CrossRef](#)] [[PubMed](#)]
13. Valderrama, J.O.; Sanga, W.W. Critical Properties and Vapor Pressure of Twenty Imidazolium based Ionic Liquids used in Extraction Bioprocesses. In Proceedings of the 2nd International Symposium on Biothermodynamics, Frankfurt am Main, Germany, 21–22 February 2008; pp. 1–9.
14. Yasui, K.; Tuziuti, T.; Kanematsu, W. Extreme conditions in a dissolving air nanobubble. *Phys. Rev. E* **2016**, *94*, 1–13. [[CrossRef](#)] [[PubMed](#)]
15. Fröba, A.P.; Rausch, M.H.; Krzeminski, K.; Assenbaum, D.; Wasserscheid, P.; Leipertz, A. Thermal conductivity of ionic liquids: Measurement and prediction. *Int. J. Thermophys.* **2010**, *31*, 2059–2077. [[CrossRef](#)]
16. Hezave, A.Z.; Raeissi, S.; Lashkarbolooki, M. Estimation of thermal conductivity of ionic liquids using a perceptron neural network. *Ind. Eng. Chem. Res.* **2012**, *51*, 9886–9893. [[CrossRef](#)]
17. Sivasankar, T.; Moholkar, V.S. Physical insights into the sonochemical degradation of recalcitrant organic pollutants with cavitation bubble dynamics. *Ultrason. Sonochem.* **2009**, *16*, 769–781. [[CrossRef](#)] [[PubMed](#)]
18. Yasui, K. Alternative model of single-bubble sonoluminescence. *Phys. Rev. E* **1997**, *56*, 6750–6760. [[CrossRef](#)]
19. Diebold, J.P. A unified, global model for the pyrolysis of cellulose. *Biomass Bioenergy* **1994**, *7*, 75–85. [[CrossRef](#)]
20. Ye, L.; Zhu, X. Analysis of the effect of impact of near-wall acoustic bubble collapse micro-jet on Al 1060. *Ultrason. Sonochem.* **2017**, *36*, 507–516. [[CrossRef](#)]
21. Avila, S.R.G.; Song, C.; Ohl, C.-D. Fast transient microjets induced by hemispherical cavitation bubbles. *J. Fluid Mech.* **2015**, *767*, 31–51. [[CrossRef](#)]
22. Schramm-Baxter, J.; Mitragotri, S. Needle-free jet injections: Dependence of jet penetration and dispersion in the skin on jet power. *J. Control. Release* **2004**, *97*, 527–535. [[CrossRef](#)] [[PubMed](#)]

Disclaimer/Publisher’s Note: The statements, opinions and data contained in all publications are solely those of the individual author(s) and contributor(s) and not of MDPI and/or the editor(s). MDPI and/or the editor(s) disclaim responsibility for any injury to people or property resulting from any ideas, methods, instructions or products referred to in the content.